Hindawi
Geofluids
Volume 2021, Article ID 6675984, 11 pages
https://doi.org/10.1155/2021/6675984

Research Article

Effects of Water Immersion on the Long-Term Bearing Characteristics of Crushed Gangue in Goaf

Ning Jiang[1], **Dawei Yin**[1], **Junbiao Ma**[1], **Liu Han**[2], **Haiyang Pan**[1,3] and **Qian Yin**[4]

[1]*State Key Laboratory of Mine Disaster Prevention and Control, Shandong University of Science and Technology, Qingdao 266590, China*
[2]*Shandong Provincial Geo-Mineral Engineering Exploration Institute, Jinan 250014, China*
[3]*General Institute of Exploration and Research of China National Administration of Coal Geology, Beijing 10039, China*
[4]*State Key Laboratory for Geomechanics and Deep Underground Engineering, China University of Mining and Technology, Xuzhou 221116, China*

Correspondence should be addressed to Ning Jiang; jiangning@sdust.edu.cn and Dawei Yin; 949251142@qq.com

Received 5 December 2020; Revised 21 December 2020; Accepted 26 February 2021; Published 12 March 2021

Academic Editor: Maurizio Barbieri

To study the long-term bearing characteristics of crushed gangue in goaf under water immersion conditions, the creep test of the crushed gangue in the water immersion state was performed by using the self-developed large-scale deformation-seepage test system of crushed rock. The effects of the rock lithology, axial stress, and grain composition on the long-term bearing deformation characteristics and fractal characteristics of crushed gangue under water immersion were analysed. The results show that under certain conditions of axial stress and grain composition of the gangue, a greater uniaxial compressive strength of water-saturated rock corresponds to a greater deformation resistance of the rock, smaller strain and crushing expansion in the corresponding creep stage, and greater fractal dimension increments of the crushed gangue after compression, and the gangue will have more serious crushing. With identical grain compositions and with the increase in the axial stress in the creep stage, the strain increases, the crushing expansion decreases, the fractal dimension increments of the crushed gangue after compression increase, and the gangue will have more serious crushing. Under identical axial stress conditions, when the Talbol power index n is 0.5, the differentials of the strain and crushing expansion for the crushed sandstone sample in the creep stage are minimal. When n is 0.3 or 0.7, these quantities are basically equal. With the increase in the Talbol power index, the fractal dimension increments of the crushed sandstone sample during compression gradually increase, and the crushed sandstone sample will have more serious crushing.

1. Introduction

After coal mining, many mined-out spaces are formed underground, which causes strata movement, damage, surface subsidence, and collapse [1–5]. Simultaneously, a large quantity of solid wastes such as gangue is discharged in the coal mining process [6–10]. Gangue discharge and surface subsidence control are common problems in coal mining. For a long time, the technology of gangue backfilling mining has developed into an effective means to control the strata movement and surface subsidence and has been widely applied [11–17]. The gangue of the main component in filling body of goaf [18, 19] is in a state of long-term pressure deformation, and its long-term bearing characteristics determine the stability of the overlying strata and filling effect of the goaf [20–23]. After the underground space is mined by filling, the filling body will face a complex geological environment. If the groundwater level changes and the water-conducting fracture zone is transfixion, the filling body may be immersed for a long time [24, 25]. Therefore, it is necessary to study the long-term bearing characteristics of the gangue filling body in a water immersion environment.

Domestic and foreign research scholars have conducted a lot of research on the long-term bearing characteristics of gangue backfilling mining. Wang et al. [26] proposed a revised relative dilatancy index for rockfill material to

describe the change in shear strength with the intermediate principal stress. The relationship among the incremental friction angle, maximum dilatancy angle, and b-value was established. Liu et al. [27] applied the crushable agglomerate method to model soil particles. Then, a series of true triaxial compression tests was performed to study the effects of the initial confining stress and intermediate principle stress on the macroscopic responses and particle breakage. Zha et al. [28] considered the grading characteristics of coal gangue and performed a field test of the screening method for coal gangue. The theory of continuous grading is used to optimize the gradation of gangue. The compressive properties of gangue with different grading indices are significantly different when the pressure is low. Huang et al. [29] studied the movement law of gangue particles with different gradations under different confining pressure conditions and loads. PFC3D shows that the shape of the coal gangue is an irregular convex polyhedron. When it is compressed, a huge contact force will be generated among the particles, which results in a chain effect. Li et al. [30] studied the compaction characteristics of 5 commonly used materials in the solid filling mining technology and found that the compaction process experienced 3 stages: rapid compaction, slow compaction, and stable compaction, and the compressive capacity of filling materials mainly depends on the particle size and strength. Li et al. [31, 32] studied the macrodeformation and particle breakage characteristics of crushed gangue through cyclic loading and unloading and continuous loading, and they revealed the mechanism of particles on the macrodeformation of crushed gangue granular materials. The results showed that the crushing ratio increased with the increase in the number of cyclic loading times, and the cyclic loading and unloading significantly improved the deformation resistance of crushed gangue. Li et al. [33] studied the energy evolution principle of coal gangue by using a self-designed experimental device and a calculation method of the coal gangue energy, and they found that the particle size had an important effect on the energy evolution of coal gangue. Zhang et al. [34] studied the pressure deformation characteristics of large-size crushed rock using a self-developed large-scale crushed rock compression deformation test system (inner diameter: 400 mm). Yu et al. [35] studied the compression samples of saturated crushed rocks with different lithology using a self-developed crushing rock compression device (inner diameter: 100 mm) and analysed the compression deformation and fractal characteristics of the samples, which were affected by 4 factors: lithology, axial stress, particle size ratio, and loading rate.

Previous scholars have made great contributions to the study of the long-term bearing capacity of crushed gangue. However, the existing test equipment is relatively simple, the diameter of the test cylinder is small, and there is a boundary effect in the test process. Therefore, the deformation-seepage experimental system of large-scale crushed gangue is used. The diameter of the test cylinder is 300 mm, and the maximum allowable particle size of crushed gangue is 60 mm. The effects of the lithology, axial stress, and grain composition on the long-term bearing deformation and fractal characteristics of gangue under water immersion are analysed. The test uses a sample that has been soaked in water for 72 h [36, 37].

2. Test Equipment and Scheme

2.1. Testing System. The experiment is performed with large-scale deformation-seepage test system of crushed rock. The system is mainly composed of the main bearing bracket, a test cylinder, a loading pressure head, a double-control servo system of the water pressure and water quantity, and a double-control servo system of the displacement and stress. The maximum axial pressure is 600 kN, and the accuracy is 0.01 kN. The main structure is shown in Figure 1. To reduce the boundary effect on the test results, the inner diameter of the test cylinder is designed to be 300 mm, the external diameter is 320 mm, and the material is 45# steel. To better simulate the state of immersion, the test system was reformed, and a water head maintaining device based on the U-tube principle was added, which can make the water head always identical to the crushed rock sample in the test process.

2.2. Test Specimen. In this experiment, four types of crushed gangues (mudstone, sandy mudstone, limestone, and sandstone) are selected to study the long-term bearing characteristics under the water immersion condition. The basic mechanical properties are shown in Table 1.

First, the four types of rocks are crushed by a crusher and sieved into 6 particle size ranges of 0-10 mm, 10-20 mm, 20-30 mm, 30-40 mm, 40-50 mm, and 50-60 mm. To overcome the disaster of dimension, the samples in this test are prepared by continuous gradation.

The Talbol continuous grading equation is used to mix the crushed rock mass of each particle size range of the sample [39] as follows:

$$P = \left(\frac{d}{D}\right)^n, \tag{1}$$

where n is the test index, D is the particle size of the crushed rock (mm), and P is the percentage of mass of the rock whose particle size is less than d in the total mass of a single sample.

To study the effect of the particle size ratio on the long-term bearing deformation and fractal characteristics of crushed gangue, the selected values of n are 0.3, 0.5, and 0.7. Under different Talbol power index conditions, the proportion of rock particles in different particle size ranges is shown in Figure 2. As the value of n increases, the content of large-size gangue increases.

2.3. Test Scheme. To study the effect of the lithology, axial stress, and grain composition on the long-term bearing deformation and fractal characteristics for crushed gangue under water immersion, 11 groups of test schemes were designed. The test scheme is shown in Table 2. Considering the discreteness of the data, the same test was repeated 3 times, and the average value of the 3 tests is taken as the test result.

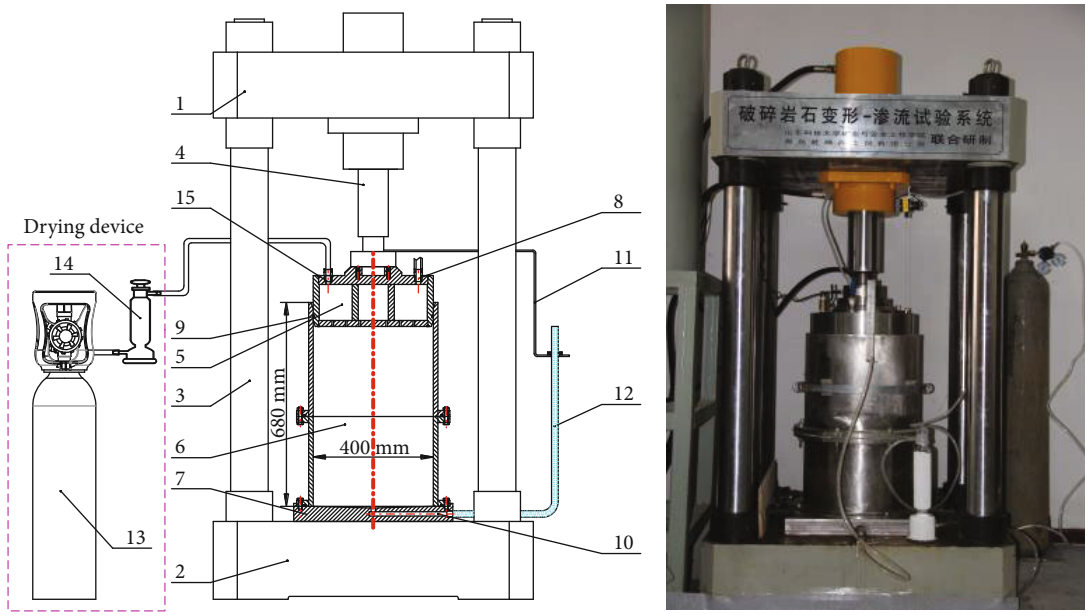

Figure 1: Deformation-seepage experimental system for crushed gangues [38]. 1: beam of the test system; 2: bedplate of the test system; 3: column; 4: load cylinder; 5: loading pressure head; 6: test cylinder; 7: bedplate of the test cylinder; 8: intake; 9: seal ring; 10: outlet; 11: fixing trestle; 12: blowout; 13: nitrogen cylinder; 14: drying tower; 15: air inlet.

Table 1: Physicomechanical parameters of rock.

Lithology	Density (g·cm^{-3})	Tensile strength (MPa)	Uniaxial compressive strength (MPa)	Elastic modulus (GPa)	Cohesion (MPa)	Internal friction angle (°)
Mudstone	2.566	1.01	15.7	8.2	7.45	19.3
Sandy mudstone	2.594	4.25	67.8	15.6	19.30	34.2
Limestone	2.578	7.46	112.9	20.2	21.56	22.75
Sandstone	2.611	8.87	107.4	32.5	32.00	38.7

2.4. Sample Method and Procedure. The creep test of crushed rock in the water immersion state uses a sample that was soaked in water for 72 h. The maintenance device of water head is used in the test, so that the water head is always at identical height to the crushed rock sample in the test process.

Due to the range of the displacement gauge and estimated maximum deformation, the control height before compressing the crushed rock is determined to be 630 mm. The prepared samples of crushed rock under water immersion are loaded into the test cylinder to the designed height, and data are collected according to the interval time required by the geotechnical test regulations [37]. The stability standard of the test is that the difference in strain is less than 5×10^4 in one hour, and the loading mode is load control. To make the stress process of crushed rock more similar to that of caving gangue in the goaf, the loading rate is 0.5 kN/s and the test loads are 1.5 MPa, 3.5 MPa, 5.5 MPa, and 7.5 MPa, respectively.

2.5. Calculation Method of the Fractal Dimension of Caving Crushed Rock. In Reference [35], the formula is the ratio of the mass of crushed gangue particles with particle size less than d in the sample to the total mass of the sample when the minimum particle size of crushed gangue is 0.

$$\frac{M_d(x<d)}{M_t} = \left(\frac{d}{d_M}\right)^{3-D}. \quad (2)$$

From equation (2), the slope of the straight line of $\lg(M_d/M_t) - \lg(d/d_M)$ is "$3-D$," and fractal dimension D of the crushed gangue sample can be calculated according to the screening results of the crushed gangue sample.

3. Analysis of the Test Results

3.1. Long-Term Bearing Deformation and Fractal Characteristics of Crushed Gangue with Different Lithology. Figures 3 and 4 show the time correlation curves of the amount of compression and strain and correlation curves of the crushing expansion and void fraction for caving crushed rock samples of different lithology under the water immersion state.

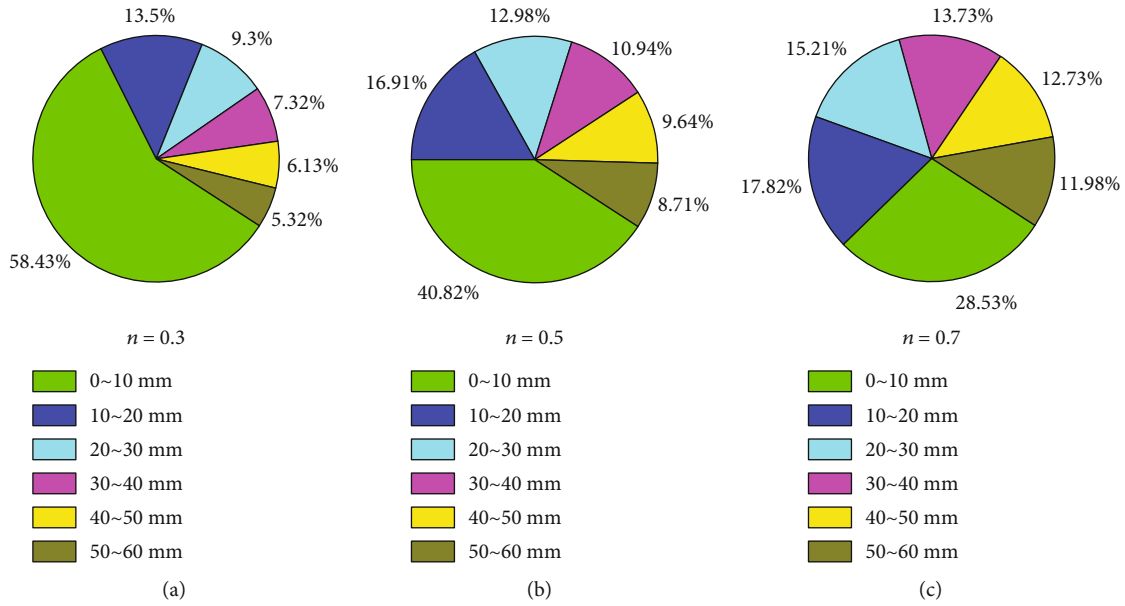

Figure 2: Grain size distribution of crushed rock for different Talbol power indices.

Table 2: Test scheme.

Test number	Lithology	Axial stress (MPa)	Talbol power exponent
JS1	Mudstone	3.5	0.5
JS2	Sandy mudstone	3.5	0.5
JS3	Limestone	3.5	0.5
JS4	Sandstone	3.5	0.5
JS5	Sandstone	1.5	0.5
JS6	Sandstone	3.5	0.5
JS7	Sandstone	5.5	0.5
JS8	Sandstone	7.5	0.5
JS9	Sandstone	3.5	0.3
JS10	Sandstone	3.5	0.5
JS11	Sandstone	3.5	0.7

Figures 3(a) and 3(b) show that the variation characteristics of the eigenvalues of deformation (amount of compression and strain) in the creep deformation stage of the caving crushed rock samples in the water immersion state correspond to the instantaneous creep stage (stage I) and stable creep stage (stage II). The eigenvalues of deformation (amount of compression and strain) are logarithmic functions of time. The more water-saturated rocks have greater uniaxial compressive strength (mudstone < sandy mudstone < sandstone < limestone) and smaller eigenvalues of deformation (amount of compression and strain) in the stable creep. Under identical axial stress, the more water-saturated rocks have greater uniaxial compressive strength and smaller differentials for the eigenvalues of deformation (differentials of the amount of compression and differentials of strain) of crushed sandstone samples in the creep deformation stage because the larger uniaxial compressive strength of water-saturated rock corresponds to greater deformation resistance.

Figures 4(a) and 4(b) show that the variation characteristics of the eigenvalues of compaction (residual crushing expansion and void fraction) in the creep deformation stage of caving crushed rock samples in the water immersion state correspond to the instantaneous creep stage (stage I) and stable creep stage (stage II), and the eigenvalues of compaction (residual crushing expansion and void fraction) are logarithmic functions of time. The more water-saturated rocks have greater uniaxial compressive strength (mudstone < sandy mudstone < sandstone < limestone) and smaller eigenvalues of compaction (residual crushing expansion and void fraction) in the stable creep. Under identical axial stress, the more water-saturated rocks have greater uniaxial compressive strength and smaller differentials for eigenvalues of compaction (differentials of residual crushing expansion and differentials of void fraction) of crushed sandstone samples in the creep deformation stage because the greater uniaxial compressive strength of rock corresponds to greater deformation resistance of rock grains.

Table 3 shows the mass distribution, fractal dimension (D), and fractal dimension increments (ΔD) of rock particles in each particle size range before and after compression for caving crushed rock samples of different lithology in the water immersion state. Figure 5 shows the variation of fractal dimension for caving crushed rock samples of different lithology before and after compression under water immersion according to Table 3.

Figure 5 shows that under identical axial stress, the more water-saturated rocks have smaller uniaxial compressive strength and greater fractal dimension increments of the

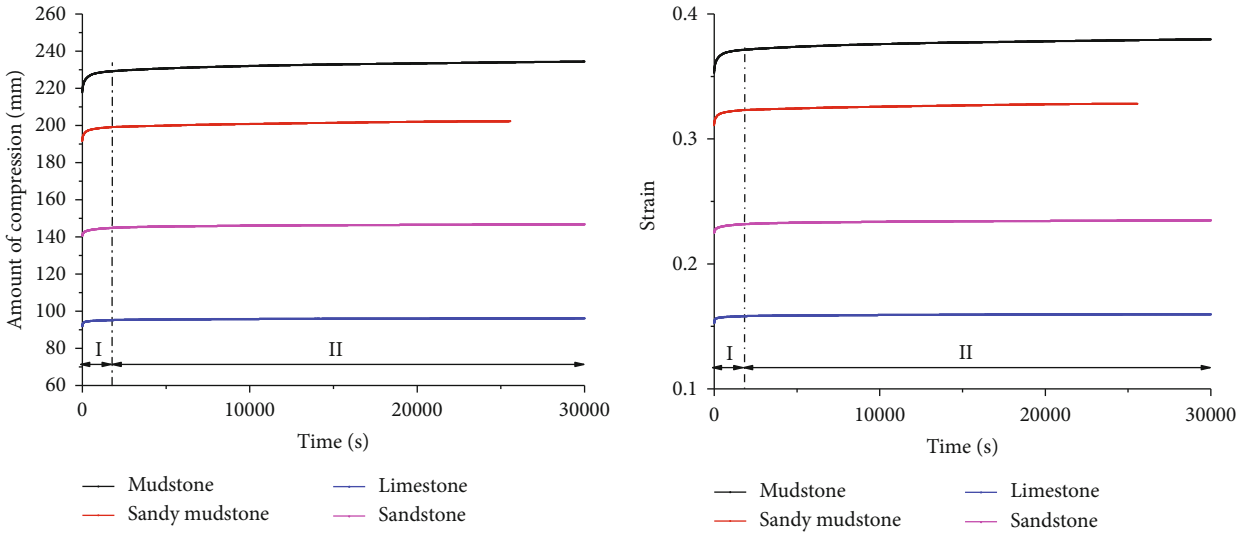

(a) Time correlation curves of the amount of compression

(b) Time correlation curves of the strain

Figure 3: Time correlation curves of the amount of compression and strain for caving crushed rock samples of different lithology (axial stress of 3.5 MPa).

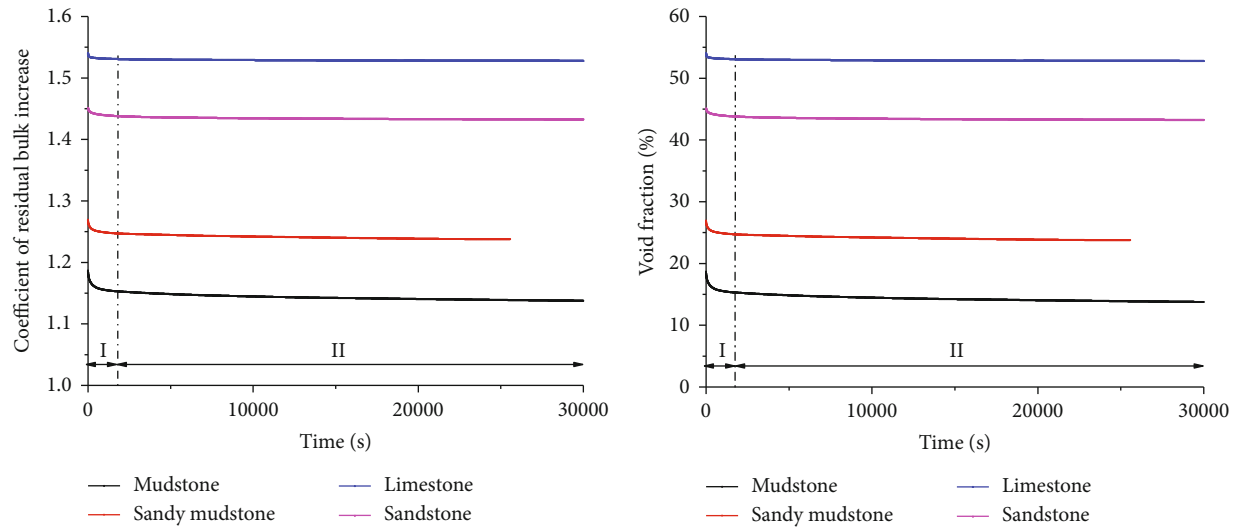

(a) Time correlation curves of the residual crushing expansion

(b) Time correlation curves of the void fraction

Figure 4: Time correlation curves of the amount of residual crushing expansion and void fraction for caving crushed rock samples of different lithology (axial stress of 3.5 MPa).

crushed gangue after compression, and the gangue will have more serious crushing. The reason is that the lower strength of the rock corresponds to worse deformation resistance, so the rock is more easily crushed.

3.2. Long-Term Bearing Deformation and Fractal Characteristics of Crushed Gangue under Different Axial Stresses. Figures 6 and 7 show the time correlation curves of the amount of compression and strain and correlation curves of crushing expansion and void fraction for caving crushed rock samples of different axial stresses under the water immersion state.

Figures 6(a) and 6(b) show that the variation characteristics of the eigenvalues of deformation (amount of compression and strain) in the creep deformation stage of the caving crushed rock samples of different axial stresses in the water immersion state correspond to the instantaneous creep stage (stage I) and stable creep stage (stage II), and the eigenvalues of deformation (amount of compression and strain) of different axial stresses are logarithmic functions of time. When the creep is stable, the eigenvalues of deformation (amount of compression and strain) increase with the increase in axial stress, and differentials for the eigenvalues of deformation of the adjacent two-stage load

Table 3: Grain size distribution and fractal dimensions of crushed rock of different lithology before and after compression (axial stress of 3.5 MPa).

Lithology	State	Quality (kg)						D	(ΔD)
		0~10 mm	10~20 mm	20~30 mm	30~40 mm	40~50 mm	50~60 mm		
Mudstone	Before compression	25.31	10.48	8.05	6.78	5.98	5.40	2.5000	0.2041
	After compression	37.04	12.73	8.26	3.19	0.78	0	2.7041	
Sandy mudstone	Before compression	25.31	10.48	8.05	6.78	5.98	5.40	2.5000	0.1662
	After compression	34.66	10.5	7.73	4.72	3.07	1.32	2.6662	
Limestone	Before compression	25.31	10.48	8.05	6.78	5.98	5.40	2.5000	0.0558
	After compression	28.36	8.74	7.50	7.42	5.56	4.42	2.5558	
Sandstone	Before compression	25.31	10.48	8.05	6.78	5.98	5.40	2.5000	0.0914
	After compression	29.68	10.16	6.98	5.37	5.32	4.50	2.5914	

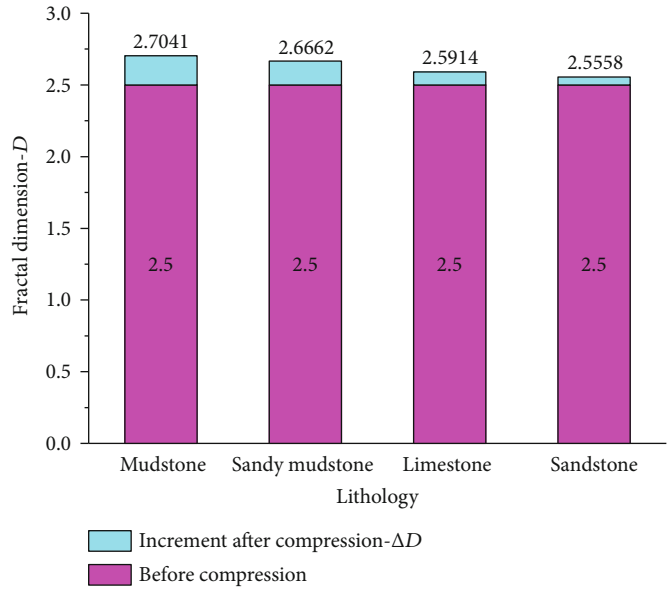

Figure 5: Variation of fractal dimensions of crushed rock samples of different lithology before and after compression (axial stress of 3.5 MPa).

decrease with the increase in load. With the increase in axial stress, the differentials of the amount of compression and differentials of strain in the creep deformation stage of the crushed sandstone samples decrease. The reason is that with the increase in axial stress, the proportion of deformation in the active loading stage caused by crushed sandstone samples under water immersion increases, and the space for creep development is relatively reduced.

Figures 7(a) and 7(b) show that the variation characteristics of eigenvalues of compaction (residual crushing expansion and void fraction) in the creep deformation stage of caving crushed sandstone samples of different axial stresses in the water immersion state correspond to the instantaneous creep stage (stage I) and stable creep stage (stage II), and the eigenvalues of compaction (residual crushing expansion and void fraction) are logarithmic functions of time. When the creep is stable, the eigenvalues of compaction (residual crushing expansion and void fraction) decrease with the increase in axial stress, and the differentials for eigenvalues of compaction (differentials for residual crushing expansion and differentials for void fraction) of the adjacent two-stage load decrease with the increase in load. With the increase in axial stress, the differentials for residual crushing expansion and void fraction in the creep deformation stage of the caving crushed sandstone samples decrease.

Table 4 shows the mass distribution, fractal dimension (D), and fractal dimension increments (ΔD) of rock particles in each particle size range before and after compression for caving crushed rock samples of different axial stresses under water immersion. Figure 8 shows the change in fractal dimension for the caving crushed sandstone samples of different axial stresses before and after compression under water immersion according to Table 4.

Figure 8 shows that with the increase in axial stress, the fractal dimension increments of the crushed sandstone sample after compression increase, and the crushed sample will have more serious crushing.

3.3. Long-Term Bearing Deformation and Fractal Characteristics of Crushed Gangue under Different Grain Compositions. Figures 9 and 10 show the time correlation curves of the amount of compression and strain and

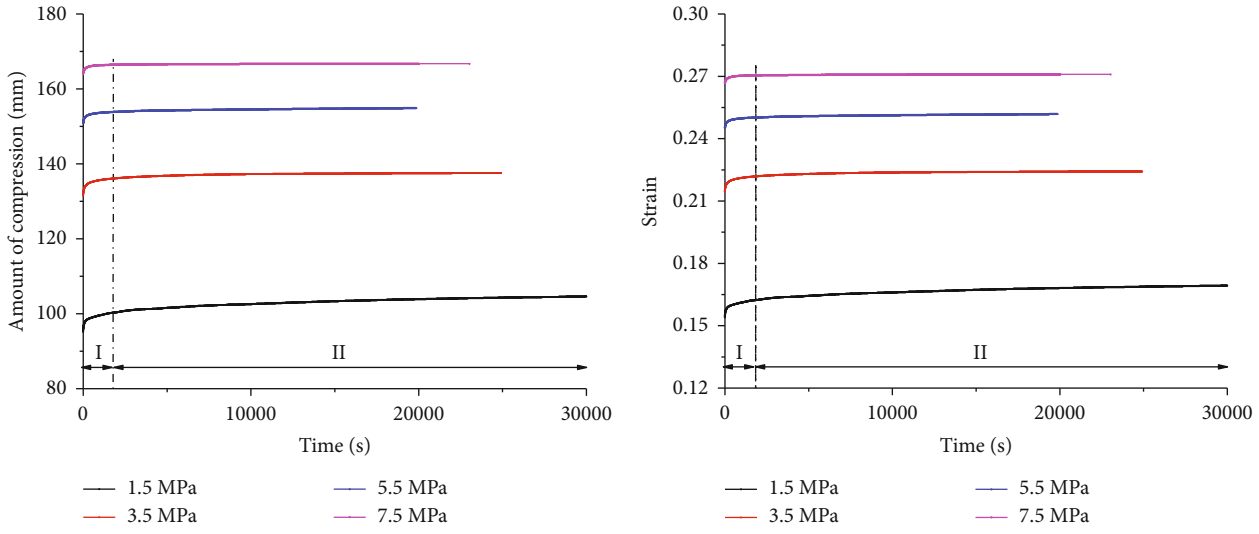

(a) Time correlation curves of the amount of compression

(b) Time correlation curves of the strain

Figure 6: Time correlation curves of the amount of compression and strain for caving crushed rock samples of different axial stresses.

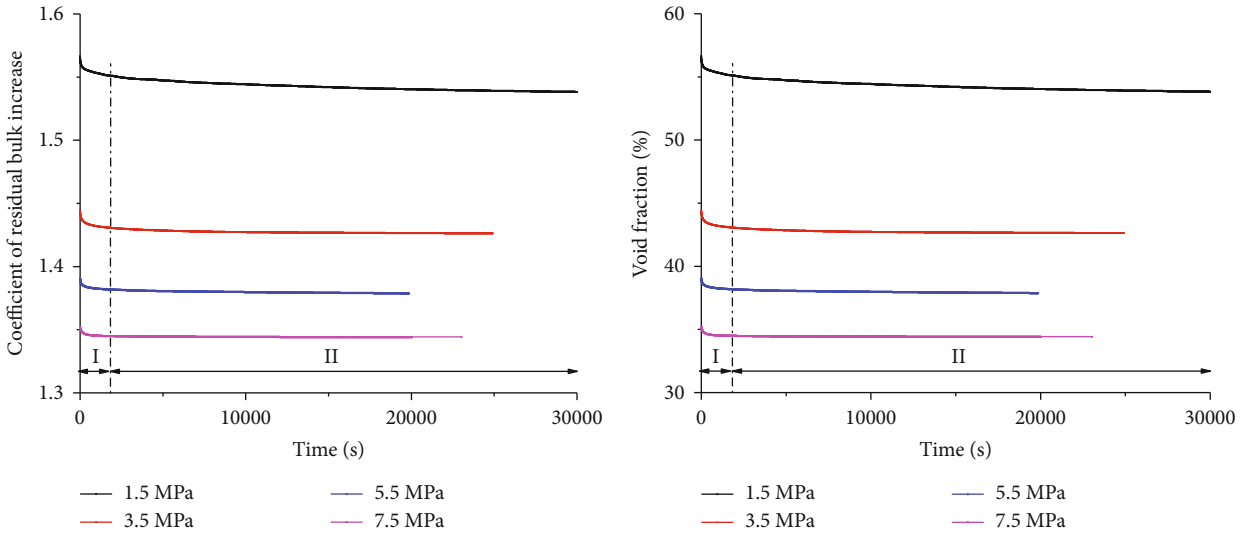

(a) Time correlation curves of the residual crushing expansion

(b) Time correlation curves of the void fraction

Figure 7: Time correlation curves of the amount of residual crushing expansion and void fraction for caving sandstone samples of different axial stresses.

Table 4: Grain size distribution and fractal dimensions of crushed sandstone samples of different axial stresses before and after compression.

Axial stress	State	Quality (kg)						D	(ΔD)
		0~10 mm	10~20 mm	20~30 mm	30~40 mm	40~50 mm	50~60 mm		
1.50 MPa	Before compression	25.31	10.48	8.05	6.78	5.98	5.40	2.5000	0.0531
	After compression	26.83	11.05	7.71	6.04	5.88	4.49	2.5531	
3.50 MPa	Before compression	25.31	10.48	8.05	6.78	5.98	5.40	2.5000	0.0914
	After compression	29.68	10.16	6.98	5.37	5.32	4.50	2.5914	
5.50 MPa	Before compression	25.31	10.48	8.05	6.78	5.98	5.40	2.5000	0.1184
	After compression	31.85	6.86	7.32	6.72	5.14	4.11	2.6184	
7.50 MPa	Before compression	25.31	10.48	8.05	6.78	5.98	5.40	2.5000	0.1481
	After compression	33.07	8.73	6.12	5.57	4.73	3.78	2.6481	

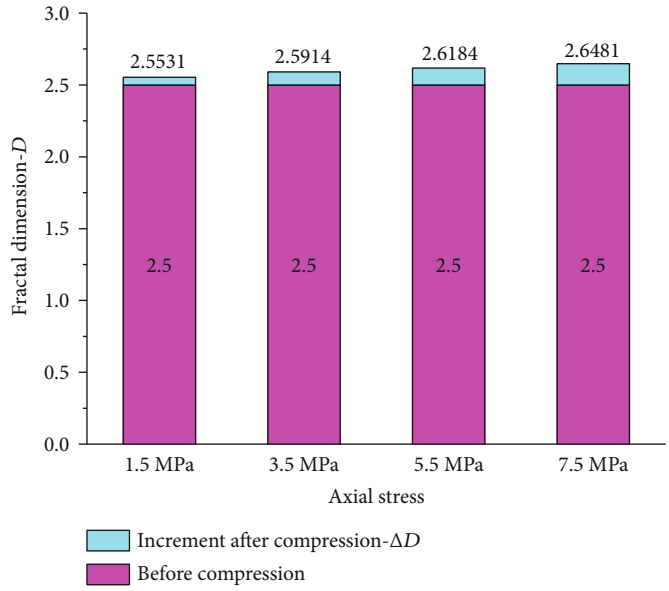

Figure 8: Change in fractal dimensions of crushed sandstone samples of different axial stresses before and after compression (axial stress of 3.5 MPa).

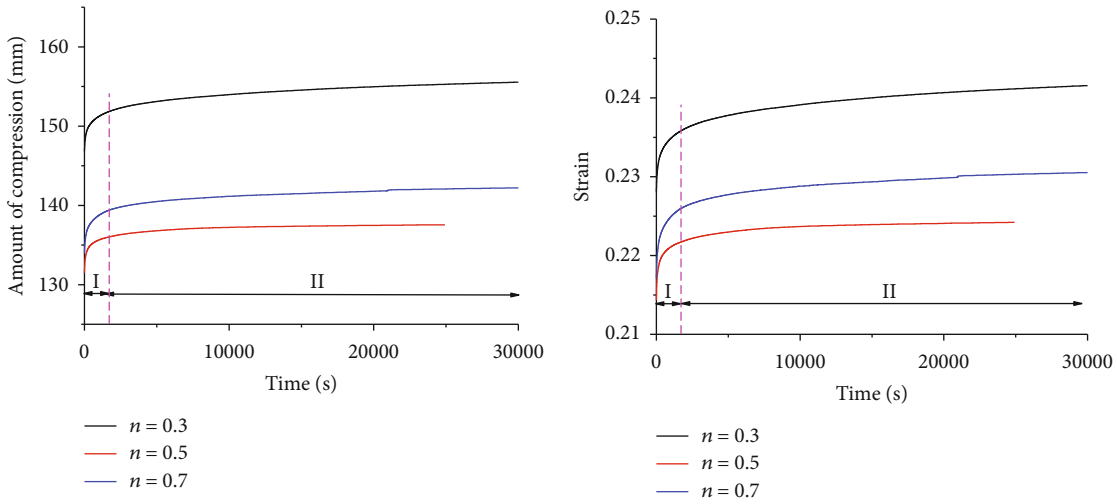

(a) Time correlation curves of the amount of compression

(b) Time correlation curves of the strain

Figure 9: Time correlation curves of the amount of compression and strain for caving crushed sandstone samples of different grain compositions (axial stress of 3.5 MPa).

correlation curves of the crushing expansion and void fraction for caving crushed sandstone samples of different grain compositions under the water immersion state.

Figures 9(a) and 9(b) show that the changes in eigenvalues of deformation (amount of compression and strain) in the creep deformation stage of the caving crushed sandstone samples with different particle size ratios in the water immersion state correspond to the instantaneous creep stage (stage I) and stable creep stage (stage II), and the eigenvalues of deformation (amount of compression and strain) are logarithmic functions of time. When the Talbol power index n is 0.5, the caving crushed sandstone samples in the stable creep stage have the smallest eigenvalues of deformation (amount of compression and strain). When n is 0.7, the eigenvalues of deformation (amount of compression and strain) are the second smallest. When n is 0.7, they are maximal. Under identical axial stress condition, when the Talbol power index n is 0.5, the crushed sandstone sample in the creep stage has the smallest differentials of compression and strain. When n is 0.5 and 0.7, these values are basically equal. The reason is that due to the softening and lubrication of water, the stress ratio (the ratio of compaction stress to rock strength) increases under identical stress conditions, so the dry density of the sample becomes the main factor that controls the deformation of the crushed sandstone samples.

Figures 10(a) and 10(b) show that the changes in eigenvalues of compaction (residual crushing expansion and void fraction) in the creep deformation stage of caving crushed

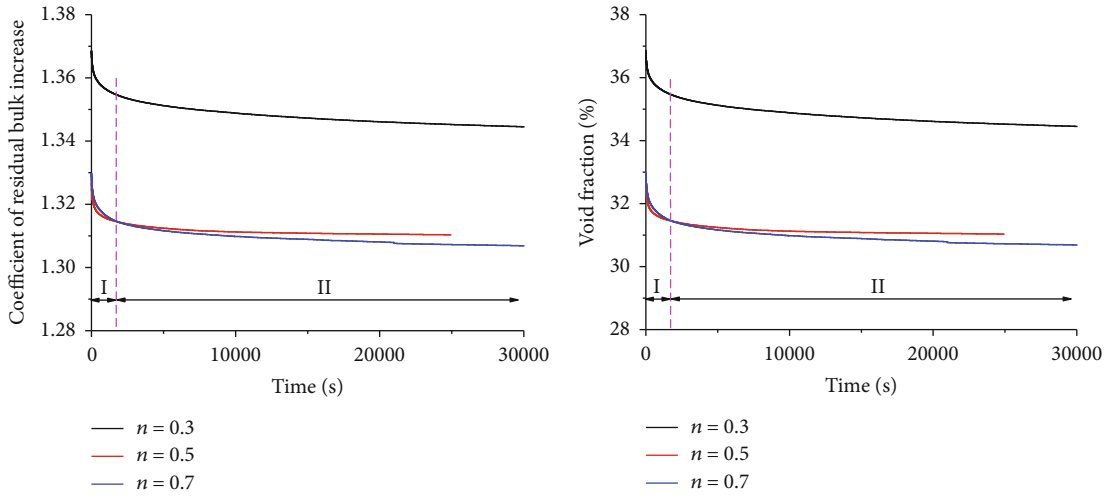

(a) Time correlation curves of the residual crushing expansion

(b) Time correlation curves of the void fraction

FIGURE 10: Time correlation curves of the amount of residual crushing expansion and void fraction for caving sandstone samples of different grain compositions (axial stress of 3.5 MPa).

TABLE 5: Grain size distribution and fractal dimensions of crushed sandstone with different grain compositions before and after compression (axial stress of 3.5 MPa).

m	State	Quality (kg)						D	(ΔD)
		0~10 mm	10~20 mm	20~30 mm	30~40 mm	40~50 mm	50~60 mm		
0.3	Before compression	36.22	8.37	5.77	4.54	3.80	3.31	2.7000	0.0338
	After compression	38.59	7.78	5.14	3.89	4.28	2.32	2.7338	
0.5	Before compression	25.31	10.48	8.05	6.78	5.98	5.40	2.5000	0.0914
	After compression	29.68	10.16	6.98	5.37	5.32	4.50	2.5914	
0.7	Before compression	17.69	11.05	9.43	8.51	7.89	7.43	2.3000	0.1766
	After compression	24.45	10.66	8.18	6.68	7.65	4.36	2.4766	

sandstone samples in the water immersion state correspond to the instantaneous creep stage (stage I) and stable creep stage (stage II), and the eigenvalues of compaction (residual crushing expansion and void fraction) are logarithmic functions of time. Under identical axial stress condition, when the Talbol power index n is 0.5, the differentials of the residual crushing expansion and void fraction for the crushed sandstone sample in the creep stage are minimal. When n is 0.5 and 0.7, these quantities are basically equal.

Table 5 shows the mass distribution, fractal dimension (D), and fractal dimension increments (ΔD) of rock particles in each particle size range before and after compression for caving crushed rock samples of different grain compositions under water immersion. Figure 11 shows the change in fractal dimension for caving crushed sandstone samples of different grain compositions before and after compression under water immersion according to Table 5.

Figure 11 shows that under identical lithology and axial stress conditions, when the Talbol power index increases, the increment of fractal dimension of the sandstone sample after compression increases, and the crushed rock particles are larger. The reason is that the larger Talbol power index corresponds to a larger proportion of large grain rock in

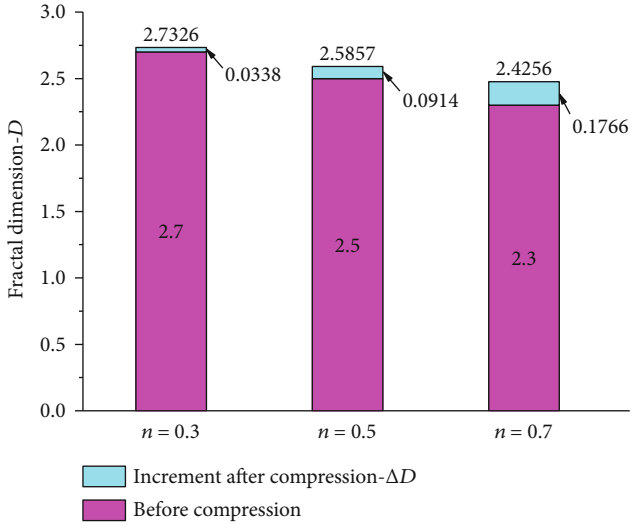

FIGURE 11: Change in fractal dimensions of the crushed sandstone samples of different grain compositions before and after compression (axial stress of 3.5 MPa).

the crushed rock sample. It is difficult for large grained rocks to roll and slide, so they are more easily crushed during compression.

4. Conclusion

Based on the long-term bearing deformation test of crushed gangue under water immersion, the effects of the gangue rock lithology, axial stress, and grain composition on the long-term bearing deformation and fractal characteristics were analysed. The main conclusions are as follows:

(1) The variation characteristics of strain of caving crushed rock samples in the creep deformation stage correspond to the instantaneous creep stage (stage I) and stable creep stage (stage II), and the eigenvalues of deformation (amount of compression and strain) are logarithmic functions of time

(2) Under certain conditions of axial stress and grain composition of gangue, if the uniaxial compressive strength of water-saturated rock increases, the deformation resistance of rock increases. Moreover, the strain and crushing expansion in the corresponding creep stage decrease, and the fractal dimension increments of the crushed gangue after compression increase, so the gangue will have more serious crushing

(3) With identical grain compositions, with the increase in axial stress in the creep stage, the strain increases, the crushing expansion decreases, the fractal dimension increments of the crushed gangue after compression increase, and the gangue will have more serious crushing

(4) Under identical axial stresses, when the Talbol power index n is 0.5, the differentials of strain and crushing expansion for the crushed sandstone sample in the creep stage are minimal. When n is 0.3 and 0.7, these quantities are basically equal. With the increase in the Talbol power index, the fractal dimension increments of crushed sandstone samples during compression gradually increase, and the crushed sandstone samples will have more serious crushing

These conclusions are of great significance to study the long-term bearing characteristics of the gangue filling body in a water immersion environment for gob gangue and traffic engineering subgrade.

Data Availability

The data used to support the findings of this study are included within the article.

Conflicts of Interest

The authors declare that there are no conflicts of interest regarding the publication of this paper.

Acknowledgments

This work was supported by the National Key R&D Program (2018YFC0604705), National Natural Science Foundation of China (52004146, 51904167, and 51774194), Taishan Scholar Talent Team Support Plan for Advantaged & Unique Discipline Areas, SDUST Research Fund (2019TDJH101), and Scientific Research Foundation of Shandong University of Science and Technology for Recruited Talents (2019RCJJ019) and Opening Fund from Key Laboratory of Mining Disaster Prevention and Control of Shandong University of Science and Technology (No. MDPC202016).

References

[1] R. Tichavský, E. Jiránková, and A. Fabiánová, "Dating of mining-induced subsidence based on a combination of dendrogeomorphic methods and in situ monitoring," *Engineering Geology*, vol. 272, article 105650, 2020.

[2] N. Jiang, C. Wang, H. Pan, D. Yin, and J. Ma, "Modeling study on the influence of the strip filling mining sequence on mining-induced failure," *Energy Science & Engineering*, vol. 8, no. 6, pp. 2239–2255, 2020.

[3] Q. Guo, X. Meng, Y. Li, X. Lv, and C. Liu, "A prediction model for the surface residual subsidence in an abandoned goaf for sustainable development of resource-exhausted cities," *Journal of Cleaner Production*, vol. 279, p. 123803, 2021.

[4] H. Liu, J. Zhang, B. Li et al., "Environmental behavior of construction and demolition waste as recycled aggregates for backfilling in mines: leaching toxicity and surface subsidence studies," *Journal of Hazardous Materials*, vol. 389, p. 121870, 2020.

[5] Z. Li, H. Zhou, D. Hu, and C. Zhang, "Yield criterion for rock-like geomaterials based on strain energy and CMP model," *International Journal of Geomechanics*, vol. 20, no. 3, article 04020013, 2020.

[6] X. X. Miao, J. X. Zhang, and M. M. Feng, "Waste-filling in fully-mechanized coal mining and its application," *Journal of China University of Mining and Technology*, vol. 18, no. 4, pp. 479–482, 2008.

[7] U. Kumarasinghe, K. Kawamoto, T. Saito, Y. Sakamoto, and M. I. M. Mowjood, "Evaluation of applicability of filling materials in permeable reactive barrier (PRB) system to remediate groundwater contaminated with Cd and Pb at open solid waste dump sites," *Process Safety and Environmental Protection*, vol. 120, pp. 118–127, 2018.

[8] C. Zhu, M. He, M. Karakus, X. Cui, and Z. Tao, "Investigating toppling failure mechanism of anti-dip layered slope due to excavation by physical modelling," *Rock Mechanics and Rock Engineering*, vol. 53, no. 11, pp. 5029–5050, 2020.

[9] D. Liu, Z. Gu, R. Liang et al., "Impacts of pore-throat system on fractal characterization of tight sandstones," *Geofluids*, vol. 2020, Article ID 4941501, 17 pages, 2020.

[10] Q. Meng, H. Wang, M. Cai, W. Xu, X. Zhuang, and T. Rabczuk, "Three-dimensional mesoscale computational modeling of soil-rock mixtures with concave particles," *Engineering Geology*, vol. 277, article 105802, 2020.

[11] F. Li, X. J. Li, L. Hou, and A. R. Shao, "A long-term study on the soil reconstruction process of reclaimed land by coal gangue filling," *Catena*, vol. 195, article 104874, 2020.

[12] J. Chen, J. Zhao, S. Zhang, Y. Zhang, F. Yang, and M. Li, "An experimental and analytical research on the evolution of mining cracks in deep floor rock mass," *Pure and Applied Geophysics*, vol. 177, no. 11, pp. 5325–5348, 2020.

[13] Z. Li, S. Liu, W. Ren, J. Fang, Q. Zhu, and Z. Dun, "Multiscale laboratory study and numerical analysis of water-weakening effect on shale," *Advances in Materials Science and Engineering*, vol. 2020, Article ID 5263431, 14 pages, 2020.

[14] H. Pan, D. Yin, N. Jiang, and Z. Xia, "Crack initiation behaviors of granite specimens containing crossing-double-flaws with different lengths under uniaxial loading," *Advances in Civil Engineering*, vol. 2020, Article ID 8871335, 13 pages, 2020.

[15] J. Li, S. Zhang, Q. Wang et al., "Feasibility of using fly ash-slag-based binder for mine backfilling and its associated leaching risks," *Journal of Hazardous Materials*, vol. 400, article 123191, 2020.

[16] Z. Li, H. Liu, Z. Dun, L. Ren, and J. Fang, "Grouting effect on rock fracture using shear and seepage assessment," *Construction and Building Materials*, vol. 242, p. 118131, 2020.

[17] W. Cai, Z. Chang, D. Zhang, X. Wang, W. Cao, and Y. Zhou, "Roof filling control technology and application to mine roadway damage in small pit goaf," *International Journal of Mining Science and Technology*, vol. 29, no. 3, pp. 477–482, 2019.

[18] Y. Wang, Y. Tan, Y. Wang, and C. Liu, "Mechanical properties and chloride permeability of green concrete mixed with fly ash and coal gangue," *Construction and Building Materials*, vol. 233, article 117116, 2020.

[19] S. Chen, Z. Du, Z. Zhang, D. Yin, F. Feng, and J. Ma, "Effects of red mud additions on gangue-cemented paste backfill properties," *Powder Technology*, vol. 367, pp. 833–840, 2020.

[20] Q. Chang, W. Tang, Y. Xu, and H. Zhou, "Research on the width of filling body in gob-side entry retaining with high-water materials," *International Journal of Mining Science and Technology*, vol. 28, no. 3, pp. 519–524, 2018.

[21] Z. Xia, N. Jiang, H. Yang et al., "Effect of multiple hole distribution and shape based on particle flow on rocklike failure characteristics and mechanical behavior," *Advances in Civil Engineering*, vol. 2020, Article ID 8822225, 13 pages, 2020.

[22] X. H. Li, W. D. Lv, Y. P. Wang, and S. S. Zhu, "Analysis of bearing mechanism and influencing factors about dual structure of pillar and filling," *Procedia Earth and Planetary Science*, vol. 1, no. 1, pp. 294–302, 2009.

[23] W. Mu, L. Li, T. Yang, G. Yu, and Y. Han, "Numerical investigation on a grouting mechanism with slurry-rock coupling and shear displacement in a single rough fracture," *Bulletin of Engineering Geology and the Environment*, vol. 78, no. 8, pp. 6159–6177, 2019.

[24] S. Chen, Z. Du, Z. Zhang, H. Zhang, Z. Xia, and F. Feng, "Effects of chloride on the early mechanical properties and microstructure of gangue-cemented paste backfill," *Construction and Building Materials*, vol. 235, article 117504, 2020.

[25] D. Yin, S. Chen, Y. Ge, and R. Liu, "Mechanical properties of rock-coal bi-material samples with different lithologies under uniaxial loading," *Journal of Materials Research and Technology*, vol. 10, pp. 322–338, 2021.

[26] Y. K. Wang, Y. F. Gao, L. Guo, and Z. X. Yang, "Influence of intermediate principal stress on the strength and dilatancy behavior of rockfill material," *Journal of Geotechnical and Geoenvironmental Engineering*, vol. 18, no. 1, article 04017128, 2018.

[27] Y. Liu, H. Liu, and H. Mao, "DEM investigation of the effect of intermediate principle stress on particle breakage of granular materials," *Computers and Geotechnics*, vol. 84, pp. 58–67, 2017.

[28] J. F. Zha, G. L. Guo, Q. Wang, and Z. G. Ma, "Study of in-situ sieving experiment and gradation optimization of gangue," *Procedia Earth and Planetary Science*, vol. 1, no. 1, pp. 754–759, 2009.

[29] Y. Huang, J. Li, Y. Teng et al., "Numerical simulation study on macroscopic mechanical behaviors and micro-motion characteristics of gangues under triaxial compression," *Powder Technology*, vol. 320, pp. 668–684, 2017.

[30] M. Li, J. X. Zhang, and X. X. Miao, "Experimental investigation on compaction properties of solid backfill materials," *Mining Technology*, vol. 123, no. 4, pp. 193–198, 2014.

[31] J. Li, Y. Huang, Z. Chen, J. Zhang, H. Jiang, and Y. Zhang, "Characterizations of macroscopic deformation and particle crushing of crushed gangue particle material under cyclic loading: in solid backfilling coal mining," *Powder Technology*, vol. 343, pp. 159–169, 2019.

[32] J. Li, Y. Huang, Z. Chen, M. Li, M. Qiao, and M. Kizil, "Particle-crushing characteristics and acoustic-emission patterns of crushing gangue backfilling material under cyclic loading," *Minerals*, vol. 8, no. 6, p. 244, 2018.

[33] M. Li, J. Zhang, N. Zhou, and Y. Huang, "Effect of particle size on the energy evolution of crushed waste rock in coal mines," *Rock Mechanics and Rock Engineering*, vol. 50, no. 5, pp. 1347–1354, 2017.

[34] J. W. Zhang, H. L. Wang, S. J. Chen, and Y. Li, "Bearing deformation characteristics of large-size broken rock," *Journal of the China Coal Society*, vol. 43, no. 4, pp. 1000–1007, 2018.

[35] B. Yu, Z. Chen, and J. Wu, "Experimental study on compaction and fractal characteristics of saturated broken rocks with different initial gradations," *Journal of Mining and Safety Engineering*, vol. 33, no. 2, pp. 342–347, 2016.

[36] J. Q. Guo, X. L. Liu, and C. S. Qiao, "Experimental study of mechanical properties and energy mechanism of karst limestone under natural and saturated states," *Chinese Journal of Rock Mechanics and Engineering*, vol. 33, no. 2, pp. 296–308, 2014.

[37] J. T. Li, R. Q. Chang, and M. P. Huang, "Creep properties of transversely isotropic slate under water-saturated and dry conditions," *Journal of Hunan University*, vol. 45, no. 5, pp. 143–148, 2018.

[38] N. Jiang, D. W. Yin, Y. J. Yang, J. B. Ma, and Y. Ge, "Experimental study on long-term load-bearing deformation and fractal characteristics of crushed gangue under dry-wet cycles," *Journal of Mining and Safety Engineering*, vol. 37, no. 1, pp. 176–182, 2020.

[39] W. S. Feng and Z. Zheng, "Tests and researches on engineering properties of large particle size fillers," *Technology of Highway and Transport*, vol. 1, 2004.